Engineered Science
DOI: https://dx.doi.org/10.30919/es1917

Preparation of a Non-Toxic Bisquaternary Quaternary Ammonium Salt from Rosin and its Application in Crop Protection

Chaoji Xiong,[1,#] Bin Wu,[1,#] Zhuo Xu,[1] Kun Liang,[1] Jia Deng,[2] Wei Wu,[3,*] Zefeng Wang,[4] Qian Chen,[1,*] Xiaoping Rao[1,5] and Chunhua Wu[1,*]

Abstract

Although quaternary ammonium salts are widely used in plant antifungal agents, their toxicity and renewability remain challenges. In this study, we synthesized three types of rosin-based gemini quaternary ammonium salts (Rbs): ortho- (o-Rbs), meta- (m-Rbs) and para- (p-Rbs) gemini salts. These salts were then tested for their *in vitro* antifungal activity against various plant pathogens, including *Valsa mali*, *Phytophthora capsici*, *Fusarium graminearum*, *Fusarium oxysporum f. sp. niveum*, and *Alternaria solani*. All three quaternary ammonium salts all exhibited significant and persistent antifungal activity against the tested pathogens. Of these, m-Rbs demonstrated the strongest activity against *V. mali* (EC_{50} = 2.649 μg/mL). In *in vivo* antifungal tests, m-Rbs exhibited promising protective and therapeutic effects on apples. A combination of spectroscopic techniques, experimental results, density functional theory (DFT), and molecular docking simulations revealed that m-Rbs effectively disrupts the cell membrane structure of *V. mali*. This disruption accelerates the leakage of intracellular contents and electrolytes. Additionally, acute toxicity tests in mice revealed that the median lethal dose (LD_{50}) of m-Rbs was 6484.198 mg/kg, classifying it as nontoxic according to standard toxicity evaluation criteria. Therefore, m-Rbs is one of the most promising antifungal agents for agricultural use.

Keywords: Dehydroabietylamine; Quaternary ammonium salt; Antifungal agents; Crop protection; Density functional theory (DFT).
Received: 13 October 2025; Revised: 26 November 2025; Accepted: 02 December 2025
Article type: Research article.

1. Introduction

With the rapid development of science and technology, human activities and globalized markets have facilitated the spread of fungal diseases. This has led to the decline or extinction of certain wild species, which can also pose a major threat to global food security.[1,2] Plant fungi, especially pathogenic ones, are now recognized as posing the greatest biological risk to agricultural production. In fact, crop losses due to fungal infections in developing countries can be as high as 50% cent or more. This poses a considerable risk to the global food supply and trade.[3] According to the most recent projections issued by the United Nations, the world's population is expected to rise to 9.5 billion by 2050, and to surpass 11 billion by 2100.[4] Consequently, agricultural productivity must increase meet the global food demand. Using fungicides to control plant fungal diseases has advantages, such as rapid efficacy and operational simplicity.[5] However, the prolonged and intensive application of existing fungicides has led to resistance development in fungal pathogens.[6,7]

Rosin is a highly abundant and renewable forest resource, and large quantities of dehydroabietic acid can be obtained from unevenly cracked rosin.[8] Dehydroabietic amine (DAAm), an important derivative of dehydroabietic acid, is widely used in various fields.[9-12] or example, Wiemann *et al.* show that the amidation of the DAAm's amino group can inhibit acetylcholinesterase activity.[13] Feng et al. prepared singlet surfactants using DAAm that exhibited good cleaning properties.[14] In addition, DAAm derivatives also exhibit diverse biological activities, including anti-herpes, anti-dengue, antibacterial, and antifungal properties.[15-17] However, the poor water solubility of these rosin-based antifungal agents limits their potential applications.[18]

Quaternary ammonium salts have positively charged cations and corresponding anions, making them highly soluble

[1]*Key Laboratory of State Forestry and Grassland Administration on Highly-Efficient Utilization of Forestry Biomass Resources in Southwest China, College of Materials and Chemical Engineering, Southwest Forestry University, Kunming, Yunnan, 650224, China*
[2]*Key Laboratory for Forest Resources Conservation and Use in the Southwest Mountains of China, Ministry of Education, Southwest Forestry University, Kunming, Yunnan, 650224, China*

in water.[19] Market demand for quaternary ammonium compounds continues to grow, reaching millions of tons globally each year.[20,21] Quaternary ammonium salts have been widely applied in antimicrobial activity research. However, there are few reports on the use of small-molecule quaternary ammonium salts in antimicrobial research, with most exhibiting high or moderate toxicity.[22-24] Additionally, most of these salts are non-renewable. Our investigation revealed that most of research reports focus on the using quaternary ammonium salts derived from modified chitosan,[25-27] cellulose[28,30] or lignin[31-33] for plant antifungal applications. Although these biomass macromolecules are renewable resources, they are all linked by reversible ether bonds. It is well known that these bonds are highly unstable in acidic solutions. Consequently, when these modified compounds enter living organisms, they may degrade into various small organic molecules, which could cause serious harm to the organisms. Therefore, there is an urgent need to develop renewable, non-toxic, and stable quaternary ammonium salt-modified, small-molecule antimicrobial agents.

In light of the aforementioned results, a non-toxic rosin-based gemini quaternary ammonium salt (**Rbs**) was synthesized by combining dehydroabietic amine with quaternary ammonium salts. In this study, we synthesized ortho- (**o-Rbs**), meta- (**m-Rbs**) and para- (**p-Rbs**) substituted twin quaternary ammonium salts, which we then subjected to in vitro antifungal screening. Subsequently, these compounds were evaluated against five common plant pathogenic fungi to identify the most effective compounds, **m-Rbs**. We also compared the antifungal efficacy of these compounds with that of the commercially available small-molecule quaternary ammonium salt benzalkonium bromide (BAB).[34] The m-Rbs was further evaluated for its *in vivo* antifungal activity against *V. mali* on apple fruits to assess its potential as an agricultural fungicide. Additionally, the antifungal mechanism against *Valsa mali* was investigated through measurements of cell membrane permeability, scanning electron microscope (SEM), Transmission electron microscope (TEM), density functional theory (DFT) calculations and molecular docking. Furthermore, the potential toxicity of **m-Rbs** in humans was evaluated by toxicological studies in mice.

2. Materials and methods

2.1 Materials and instruments

Materials and equipment are detailed in the supporting information.

2.2 The synthesis of three quaternary ammonium salts

The following are the synthesis routes for three novel rosin-based bisquaternary ammonium salts (Scheme 1). In our previous work, we have successfully synthesized compound 1 (Fig. S1 and Fig. S5).[35]

A mixture containing 1.31 g of compound 1 (4.4 mmol, 2.2 eq) and 1,2-bis(bromomethyl)benzene (0.53 g, 2 mmol, 1 eq) in 20 mL of acetonitrile and 10 mL of isopropanol was heated to 86 °C. After 72 h, the solvent was then removed and the compound was purified by ethyl acetate: methanol (10:1) separation to give 0.8 g of **o-Rbs** (yield: 43%). ^{1}H-NMR (500MHz, DMSO-D_6) δ 7.85 (d, *J* = 10Hz, 2H), 7.71 (d, *J* = 5Hz, 2H), 7.13 (d, *J* = 5Hz, 2H), 6.97 (d, *J* = 10Hz, 2H), 6.87 (s, 2H), 3.62 (s, 4H), 3.13 (s, 12H), 2.91-2.84 (m, 2H), 2.79-2.77 (t, *J* = 5Hz, 4H), 2.79-2.77 (t, *J*= 5Hz, 4H), 2.26 (s, 4H), 2.04 (d, *J*=5Hz, 4H), 1.93 (d, *J* = 5Hz, 4H), 1.70-1.68 (t, J=5Hz, 4H), 1.62 (d, *J*=10Hz 4H), 1.39 (d, *J* =5Hz, 2H), 1.27 (s, 6H), 1.19 (s, 6H), 1.16 (d, *J* = 5Hz, 12H). ^{13}C-NMR (126 MHz, DMSO-D_6) 147.5, 146.7, 136.4, 134.5, 131.34, 130.2, 126.8, 124.2, 75.3, 67.2, 50.9, 48.2, 38.1, 37.6, 37.6, 33.4, 30.0, 25.8, 24.4, 19.6, 19.5, 18.5 (Fig. S2). HRMS (ESI, m/z) = 365.8104 $[M]^{2+}/2$ (Fig. S6).

The synthesis of the **m-Rbs** (0.89g, yield: 48%) and **p-Rbs** (0.79g, yield: 42%) followed the same procedure as the synthesis of the **o-Rbs**. **m-Rbs**: ^{1}H-NMR (500MHz, DMSO-D_6) δ 7.94 (s, 1H), 7.79 (d, *J* = 10Hz, 2H), 7.67-7.64 (t, 1H), 7.14 (d, *J* = 5Hz, 2H), 6.88 (s, 2H), 6.97 (d, *J* = 10Hz, 2H), 3.72 (s, 4H), 3.13 (s, 12H), 2.93-2.88 (m, 2H), 2.79-2.76 (t, *J* = 5Hz, 4H), 2.29 (s, 4H), 2.09 (d, *J* = 5Hz, 4H), 1.89 (d, *J* = 5Hz, 4H), 1.75-1.70 (t, *J* = 10Hz, 4H), 1.67 (d, *J* = 10Hz, 4H), 1.39 (d, *J* = 10Hz, 2H), 1.28 (d, 6H), 1.15 (d, *J* = 5Hz, 12H). ^{13}C-NMR (126 MHz, DMSO-D_6) 147.5, 146.7, 128.4, 126.5, 134.5, 129.4, 126.8, 124.8, 124.7, 76.8, 69.6, 51.6, 47.8, 38.1, 37.9, 37.5, 33.4, 29.7, 25.7, 24.4, 24.4, 19.6, 19.4, 18.6 (Fig. S3). HRMS (ESI, m/z) = 365.8161 $[M]^{2+}/2$ (Fig. S7). **p-Rbs**: ^{1}H-NMR (500MHz, DMSO-D_6) δ 7.19 (s, 4H), 1.15 (d, *J* = 10Hz, 2H), 6.97 (d, *J* = 5Hz, 2H), 6.87 (s, 2H), 3.72 (s, 4H), 3.11 (s, 12H), 2.93-2.88 (m, 2H), 2.79-2.76 (t, *J* = 5Hz, 4H), 2.29 (s, 4H), 2.08 (d, *J* = 10Hz, 4H), 1.90-1.86 (t, *J* = 10Hz, 4H), 1.75-1.70 (t, *J* = 10Hz, 4H), 1.65 (d, *J* = 10Hz, 4H), 1.34-1.30 (t, *J* = 10Hz, 2H), 1.27 (s, 6H), 1.20 (s, 6H), 1.15 (d, *J* = 5Hz, 12H). ^{13}C-NMR (126 MHz, DMSO-D_6) 147.6, 145.7, 134.4, 133.9, 130.8, 126.8, 124.2, 76.7, 69.6, 51.7, 51.5, 47.7, 38.1, 37.8, 37.6, 33.4, 29.8, 25.8, 24.4, 34.4, 19.9, 19.4, 18.6 (Fig. S4). HRMS (ESI, m/z) = 365.8080 $[M]^{2+}/2$ (Fig. S8).

2.3 Antifungal activity assay of three quaternary ammonium salts

We used the mycelium growth rate method to assess the in vitro antifungal activity of three quaternary ammonium salts

[3]UCL Department of Physics and Astronomy, University College London, Gower Street, London, WC1E 6BT, UK
[4]*College of Traditional Chinese Medicine, Yunnan University of Chinese Medicine, Kunming, Yunnan, 6500, PR China*
[5]*College of Chemical Engineering, Huaqiao University, Xiamen, Fujian, 361021, China*
[#]*These authors contributed equally to this work.*
[*]*Email:* wei.wu@ucl.ac.uk (Wei Wu), chenqian@hit.edu (Qian Chen), kmwuchunhua@swfu.edu.cn (Chunhua Wu)

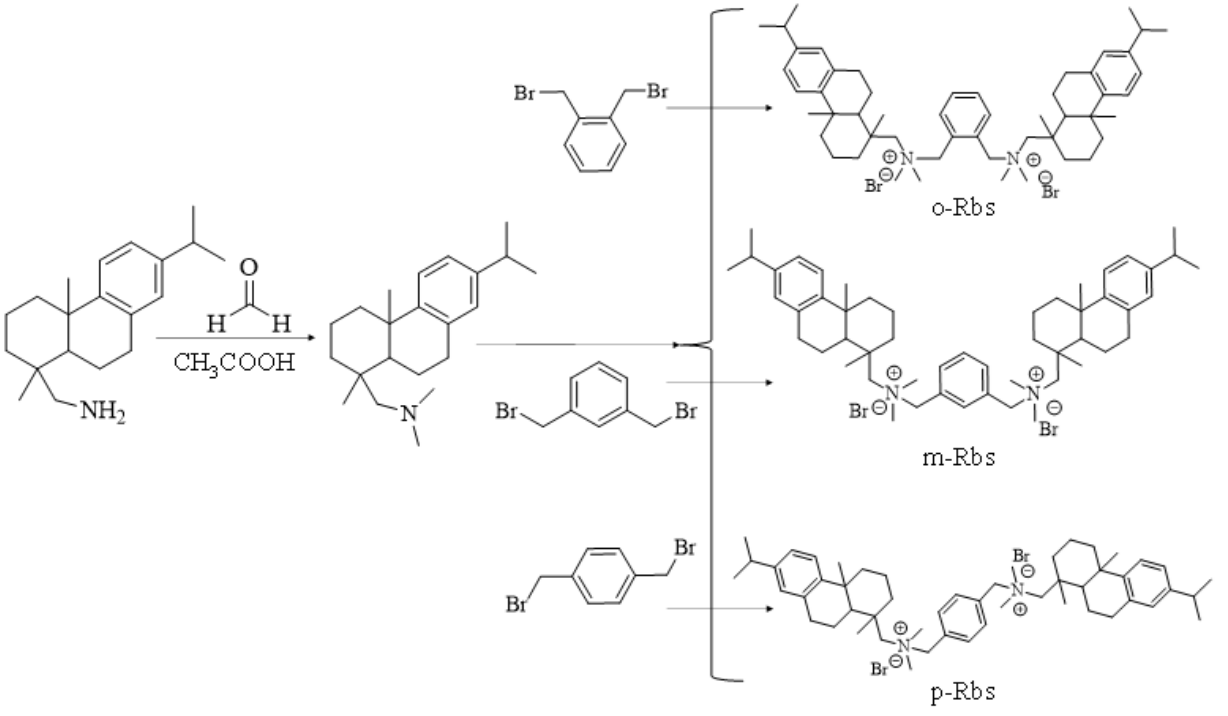

Scheme 1: Synthesis route of **o-, m-, p-Rbs**.

against the following fungi: *V. mali, P. capsica, F. graminearum, F. oxysporum f. sp. niveum,* and *A. solani*.[36] Additionally, PDA medium without any compounds served as the blank control throughout the entire experimental procedure, while medium containing an equivalent concentration of bromophenylbenzylammonium bromide (**BAB**) served as the positive control.

Preliminary in vitro antifungal tests indicated that **m-Rbs** exhibits significant inhibitory effects against *V. mali*. We therefore investigated the in vivo antifungal efficacy of **m-Rbs** against this *V. mali* on apple fruit.[37] More detailed operational support information is available.

2.4 Effects of m-Rbs compound on *V. mali*

First, the effect of **m-Rbs** on cytoplasmic cytoplasmic content leakage in *V. mali* was tested.[38,39] The procedure was as follows: 6 mm mycelial plugs were inoculated into potato dextrose (PD) liquid medium and cultured with shaking for 5 days. Subsequently, 2 g of mycelia were suspended in phosphate-buffered saline (PBS), and **m-Rbs** was added to prepare solutions with final concentrations of 50, 100, and 200 μg/mL. A compound-free PBS solution was used as a negative control, with three replicates prepared for each treatment. After 24 h of continuous shaking incubation, the absorbance of the solutions was measured at 260 nm and 280 nm to evaluate the extent of leakage of intracellular contents.

Based on established methods in the literature, the effect of **m-Rbs** on the membrane permeability of *V. mali* was evaluated.[40-42] First, 6 mm mycelial plugs were inoculated into potato dextrose (PD) liquid medium and cultured with shaking for 5 days. Subsequently, **m-Rbs** was prepared at concentrations of 50, 100, and 200 μg/mL, with a compound-free solution serving as a negative control. Three replicates were made for each treatment. Then, 0.5 g of mycelia was added to each solution, and the conductivity was monitored continuously for 12 h using a conductivity meter. The maximum conductivity value was determined by measuring the solution after boiling the mycelia. Finally, the relative permeability of the cell membrane was calculated using formula 1 to assess the extent of the effect of **m-Rbs** against *V. mali* on the integrity of the cell membrane.

$$\textit{Relative electrical conductivity}\ (\%) = (D_1\text{-}D_0)/(D_2\text{-}D_0) \times 100 \quad (1)$$

D_0 represents the conductivity of each solution at 0 h, D_1 denotes the conductivity of each sample at a given time, and D_2 corresponds to the conductivity after boiling the mycelia.

2.5 Calculation of DFT

The geometric optimization of the **m-Rbs**, and the calculation of the single-point energy, were performed using the B3LYP/6-311+G level of theory in Gaussian 09.[43,44] We have taken into account the solvation (water) effect of adsorbent by using the solvation model based on density (SMD).

2.6 Molecular docking

In this study, molecular docking was performed using Auto Dock Vina software (version 1.1.2). The crystal structures of the target proteins CYP51 (1CBJ), SOD (1TGU), POD (2X08), and CAT ($6CR_2$) were obtained from the RCSB Protein Data Bank.[45] After initial docking, the binding free energy of each complex was first calculated using Vina, followed by interaction analysis and visualization using PyMOL and Discovery Studio 2019 software.

2.7 Acute toxicity study in mice

This study evaluated the median lethal dose (LD_{50}) of **m-Rbs** using acute oral toxicity testing.[46] The feeding as well as experimental requirements in the ARRIVE guidelines were met. In initial tests, concentration gradients of **m-Rbs** were established at 0, 3125, 6250, 12500, and 25000 μg/mL. Forty ICR mice of similar body weight (40±2 g), equally divided by gender sex, were randomly assigned to five experimental groups. Treatment groups received 800 μL of the corresponding **m-Rbs** solutions by oral gavage daily, while the control group received an equivalent volume of normal saline. Survival rates were monitored daily during the 7-day observation period, and complete necropsies and organ photographs were performed immediately after mortality.

3. Result and discussion

3.1 In vitro antifungal activity analysis

Fig. S9 and Table 1 show the results of the antimicrobial tests on three quaternary ammonium salts and **BAB** (the positive control) against five plant-pathogenic fungi. The results demonstrate that **o-Rbs**, **m-Rbs** and **p-Rbs** exhibit significant broad-spectrum antifungal activity. At high concentrations, the inhibition rates of the three quaternary ammonium salts against the five plant pathogenic fungi were slightly lower than those of the positive control. However, at low concentrations, the inhibition rates of the three quaternary ammonium salts were generally higher than those of the positive control. For example, at 6.25 μg/mL, the inhibition rates of the **o-Rbs** against the aforementioned pathogens were 23.27%, 12.59%, 35.28%, 23.72%, and 11.39%, respectively. The m-Rbs showed inhibition rates of 73.41%, 31.98%, 45.79%, 51.64%, and 12.95%, respectively. The p-Rbs showed inhibition rates of 30.90%, 8.71%, 26.87%, 23.12%, and 23.92%, respectively. In comparison, the **BAB** showed inhibition rates of 51.70%, 8.18%, 18.75%, 9.92%, and 12.95%, respectively. Notably, except for the slightly lower inhibition rates of **o-Rbs** and **p-Rbs** against *V. mali* compared to **BAB**, the three quaternary ammonium salts outperformed the positive control in inhibiting the other plant pathogenic fungi.

The EC_{50} values were calculated based on the inhibition rates at different concentrations. The ortho-substituted quaternary ammonium salt (**o-Rbs**) showed EC_{50} values of 9.25, 20.984, 16.960, 17.060, and 21.719 μg/mL against *V. mali, P. capsica, F. graminearum, F. oxysporum f. sp. niveum*, and *A. solani*, respectively. The **m-Rbs** showed EC_{50} values of 2.649, 8.998, 7.025, 3.809, and 21.848 μg/mL against the aforementioned pathogens, respectively. The **p-Rbs** showed EC_{50} values of 7.374, 19.490, 15.358, 14.734, and 12.631 μg/mL against the same pathogens, respectively. In comparison, the **BAB** showed EC_{50} values of 5.982, 15.777, 25.545, 32.747, and 31.000 μg/mL, respectively. The EC_{50} values of **o-Rbs** and **p-Rbs** against *F. graminearum, F. oxysporum f. sp. niveum*, and *A. solani* were lower than those of **BAB**, while their EC_{50} values against *V. mali* and *P. capsica* were higher than those of **BAB**. Notably, **m-Rbs** exhibited lower EC_{50} values than **BAB** against all five plant pathogenic fungi, with an exceptionally low EC_{50} value of 2.649 μg/mL against *V. mali*, indicating superior antifungal activity. A comprehensive comparison of the EC_{50} values of the three quaternary ammonium salts against the five plant pathogenic fungi revealed that the **m-Rbs**, exhibited the most potent broad-spectrum antifungal activity with particularly remarkable efficacy against *V. mali*. This finding provides an important theoretical basis for the development of novel and highly effective fungicides.

Table 1: Inhibition rates and EC_{50} of three quaternary ammonium salts and benzalkonium bromide against five plant pathogenic fungi.

Average Inhibition Rate (%) ± Standard Deviation (SD, n = 3)

Compound	Concentration (μg/mL)	*V. mali*	*P. capsici*	*F. graminearum*	*F. oxysporum f. sp.niveum*	*A. solani*
o-Rbs	200	100.00±0.00	93.91±1.04	74.03±0.23	86.79±0.40	81.98±1.70
	100	99.55±0.10	85.93±0.82	72.51±0.19	83.48±0.80	78.45±1.67
	50	96.75±0.22	82.78±0.18	66.66±0.29	81.98±0.60	74.51±0.33
	25	94.53±0.72	68.52±0.14	55.64±1.51	64.86±1.80	69.41±0.24
	12.5	68.60±1.76	24.23±1.30	46.52±0.63	39.04±0.80	37.66±1.09
	6.25	23.27±0.32	12.59±0.40	35.28±1.59	23.72±0.40	11.39±1.93

Average Inhibition Rate (%) ± Standard Deviation (SD, n = 3)

Compound	Concentration (μg/mL)	*V. mali*	*P. capsici*	*F. graminearum*	*F. oxysporum f. sp.niveum*	*A. solani*
m-Rbs	EC_{50} (μg/mL)	9.525	20.984	16.960	17.060	21.719
	200	100.00±0.00	99.43±0.01	95.23±3.18	82.39±0.65	93.12±2.25
	100	100.00±0.00	98.30±0.02	89.15±2.04	79.41±0.43	82.33±1.04
	50	97.51±1.75	96.97±0.23	81.56±0.80	75.54±1.76	80.17±0.46
	25	93.58±0.21	95.06±0.45	75.28±1.16	68.67±1.53	69.23±1.00
	12.5	91.38±0.19	62.56±0.93	64.45±2.21	65.80±1.13	23.48±0.60
	6.25	73.41±2.68	31.98±2.71	45.79±2.14	51.64±0.21	12.95±0.51
p-Rbs	EC_{50} (μg/mL)	2.649	8.998	7.025	3.809	21.848
	200	97.52±0.20	93.53±0.48	77.08±0.37	81.08±0.00	77.60±0.15
	100	96.81±0.32	87.05±0.95	75.11±0.14	79.58±0.40	75.99±0.45
	50	95.74±0.06	86.48±0.22	73.15±1.23	78.68±0.40	73.61±0.44
	25	91.32±0.86	76.11±0.18	65.73±0.96	69.97±0.40	69.61±0.51
	12.5	84.68±1.32	27.04±1.02	50.01±0.87	50.15±0.80	60.80±1.53
	6.25	30.90±2.12	8.71±1.80	26.87±1.46	23.12±1.40	23.92±0.52
BAB	EC_{50} (μg/mL)	7.374	19.490	15.358	14.734	12.631
	200	100.00±0.00	100±0.00	88.13±1.42	94.89±0.76	100.00±0.00
	100	100.00±0.00	98.64±0.22	79.89±1.28	85.55±0.49	95.25±2.47
	50	100.00±0.00	95.73±1.30	66.35±0.66	69.89±1.35	66.54±2.10
	25	92.65±2.77	86.13±0.92	48.75±0.50	30.43±0.70	46.41±0.99
	12.5	79.57±3.05	26.78±1.49	34.53±0.98	19.57±0.70	10.99±1.12
	6.25	51.70±1.43	8.18±1.46	18.75±0.92	9.92±1.06	0.95±0.63
	EC_{50} (μg/mL)	5.982	15.777	25.545	32.747	31.000

To further evaluate the antifungal persistence of **m-Rbs**, its sustained inhibitory effects against the five plant pathogenic fungi were investigated (Fig. 1 and Fig. S10). A blank control group of *V. mali, P. capsica*, and *F. graminearum* grew throughout the medium on four day (Fig. S10A, Fig. S10B and Fig. S10C). During this period, at 6.25 μg/mL, the inhibition rate of **m-Rbs** against *V. mali* decreased from 73.41% on the second day to 59.49% on the fourth day, while the inhibition rates against *P. capsica* and *F. graminearum* decreased from 31.98% to 19.41% and from 45.79% to 40.19%, respectively. At the rest of the concentrations, relatively stable inhibition rates against these three fungi were maintained over the four-day period. A blank control group of *F. oxysporum f. sp. niveum* and *A. solani* grew throughout the medium on seven

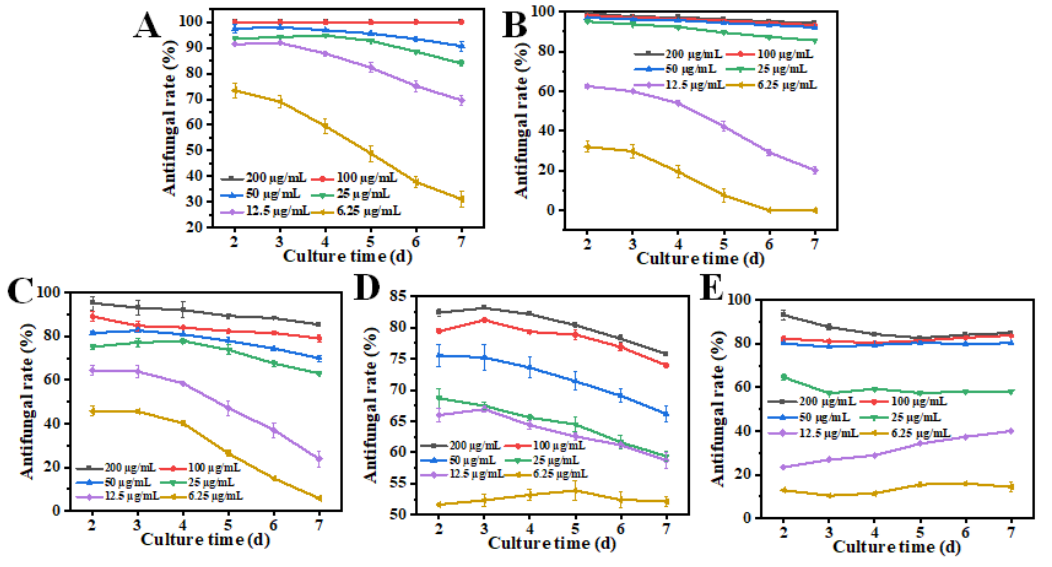

Fig. 1: Antifungal persistence of compound **m-Rbs** against *V. mali* (A), *P. capsica* (B), *F. graminearum* (C), *F. oxysporum f. sp. niveum* (D) and *A. solani* (E).

day (Fig. S10D and Fig. S10E). At this stage, **m-Rbs** showed an inhibition rate of 6.25 μg/mL against *F. oxysporum f. sp. niveum*, which remained largely unchanged. Slight decreases were observed at other concentrations. Notably, the inhibition rates of **m-Rbs** against *A. solani* remained stable or even slightly increased at all concentrations. These results demonstrate that **m-Rbs** has significant sustained inhibitory activity against the pathogenic fungi tested, providing important experimental evidence for the development of long-lasting antifungal agents.

3.2 In vivo antifungal activity analysis of m-Rbs

The protective and curative effects of **m-Rbs** on apple fruits following inoculation with *V. mali* were further investigated, with comparative evaluation against the positive control, **BAB**. As shown in Fig. 2C, both **m-Rbs** and **BAB** exhibited significant protective and curative effects on apples. Specifically, at concentrations of 50, 100, and 200 μg/mL, the protective efficacy (PE) of **m-Rbs** was 78.04%, 67.81%, and 52.14%, respectively (Fig. 2A), which was slightly lower than that of **BAB** (79.04%, 74.65%, and 61.91%). Similarly, the curative efficacy (CE) of **m-Rbs** at the same concentrations was 78.12%, 71.48%, and 58.61%, respectively (Fig. 2B), comparable to that of **BAB** (75.00%, 69.93%, and 62.69%). These results underscore the promising potential of **m-Rbs** for practical crop protection applications.

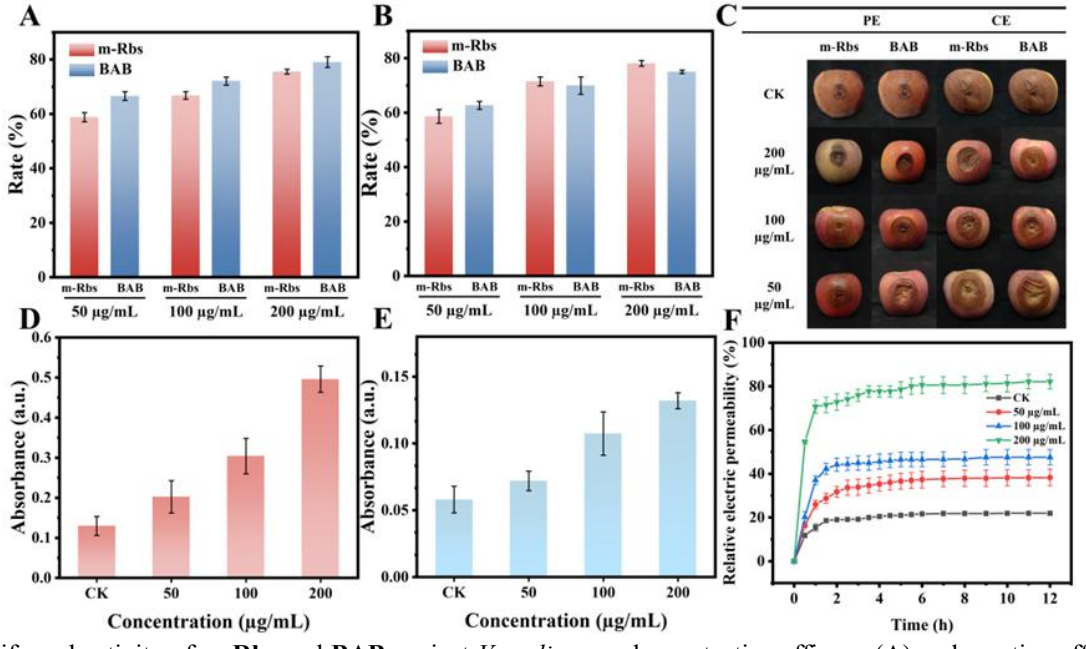

Fig. 2: The antifungal activity of **m-Rbs** and **BAB** against *V. mali* on apple: protective efficacy (A) and curative efficacy (B). The effect of the **m-Rbs** and **BAB** on the fungus *V. mali* on apples (C). Leakage content of the contents of *V. mali* after treatment with **m-Rbs**: 260 nm (D) and 280 nm (E). The effect of **m-Rbs** on the relative conductivity of *V. mali* (F).

3.3 Cytoplasmic content leakage analysis

The content of nucleic acids and proteins can be measured by their absorbance at 260 nm and 280 nm, respectively, which allows the assessment of cytoplasmic leakage.[47] As shown in Fig. 2D and 2E, the absorbance values at 260 nm were 0.130 for the blank control group and 0.202, 0.314, and 0.490 for the groups treated with 50, 100, and 200 μg/mL **m-Rbs**, respectively. At 280 nm, the absorbance values were 0.058 for the blank control group and 0.072, 0.107, and 0.132 for the groups treated with 50, 100, and 200 μg/mL **m-Rbs**, respectively. The absorbance values increased significantly with higher concentrations of **m-Rbs**, indicating a significant increase nucleic acids and proteins content in the solution. This phenomenon confirms that **m-Rbs** disrupts the integrity of the cell membrane, accelerates the leakage of intracellular contents, and leads to a reduction of nucleic acids and proteins inside the cells, thereby affecting their normal physiological functions.

3.4 The effect of m-Rbs on cell membrane permeability of *V. mali*

The cell membrane is a vital component of cells that provides a relatively stable environment and plays a critical role in cellular functions.[48,49] Fig. 2F illustrates the changes in the relative conductivity of *V. mali* cells, which were treated with 50, 100, and 200 μg/mL **m-Rbs** Eq. (1) The results show that **m-Rbs** treatment induces a distinct three-phase change in solution conductivity: a sharp increase within the first 2 h, followed by a gradual increase between 2-6 h, and finally a stabilization after 6-12 h. Furthermore, the conductivity increases more significantly at higher concentrations of the compound. These observations suggest that **m-Rbs** disrupts cell membrane integrity, increases membrane permeability, and causes substantial leakage of intracellular electrolytes, thereby interfering with normal cellular activities. The degree of damage increases with increasing concentration of the compound.

3.5 Surface morphology and ultrastructural analysis of cells

The effects of **m-Rbs** on the surface morphology of the mycelia were observed by scanning electron microscopy (SEM). Mycelia in the blank control group (Fig. 3A and 3B) showed regular and robust growth with uniform thickness, smooth surfaces, and no apparent wrinkling, twisting, or damage. In contrast, **m-Rbs**-treated mycelia (Fig. 3C and 3D) exhibited irregular and sparse growth, uneven thickness, rough surfaces, and significant dehydration-induced shrinkage and distortion. These observations suggest that **m-Rbs** disrupts the normal growth of mycelia. The effects of **m-Rbs** on cellular ultrastructure were further investigated using transmission electron microscopy (TEM). Cells in the blank control group (Fig. 3E and 3F) showed intact cell membranes and cell walls, clear borders, abundant cytoplasmic contents, and well-defined organelles, including nuclei and mitochondria, without large vacuoles or obvious cavities. In contrast, **m-Rbs**-treated cells (Fig. 3G and 3H) showed plasmolysis, blurred cell borders, dissolved plasma membranes, disintegrated and unrecognizable organelles, and the presence of numerous vacuoles and cavities. These ultrastructural changes suggest that **m-Rbs** is likely to disrupt normal cellular physiological functions by compromising the integrity of cell membranes and organelles.

3.6 DFT analysis

The electronic properties of **m-Rbs** were investigated by density functional theory (DFT) calculations. The energy gap between the highest occupied molecular orbital (HOMO) and the lowest unoccupied molecular orbital (LUMO) was determined to be 3.01 eV (Fig. 4A), indicating significant chemical reactivity. In addition, the DFT-derived molecular electrostatic potential (MEP) mapping (Fig. 4B) revealed that the strongest electrostatic potentials localized in the quaternary ammonium group and bromine atom regions. in **m-Rbs** structure would preferentially form hydrogen bonds with either the hydrogen atoms of amino groups or carboxyl groups. It is hypothesized that these interactions could potentially disrupt protein synthesis and compromise membrane integrity.

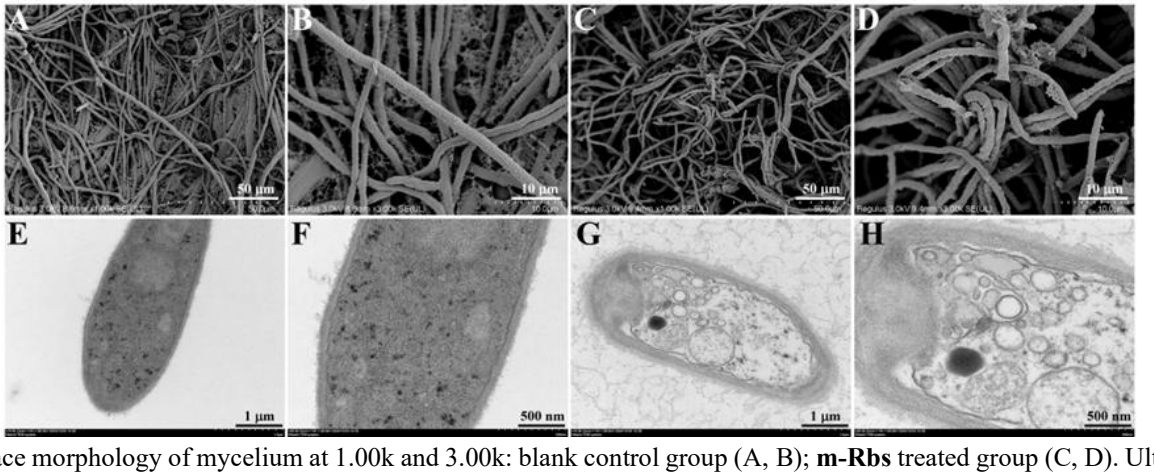

Fig. 3: Surface morphology of mycelium at 1.00k and 3.00k: blank control group (A, B); **m-Rbs** treated group (C, D). Ultrastructure of mycelium at 15.0k and 30.0k: blank control group (E, F); **m-Rbs** treated group (G, H).

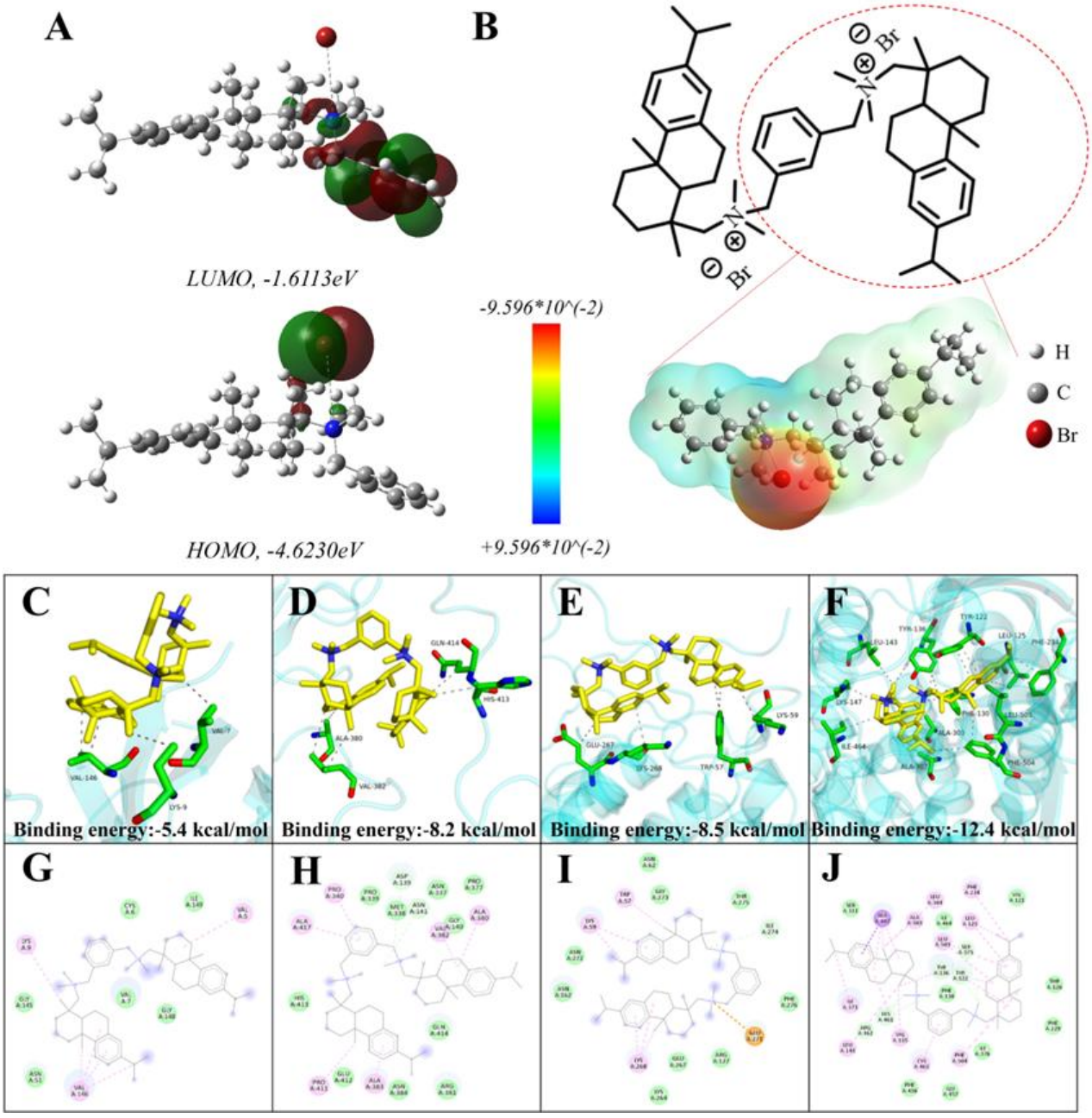

Fig. 4: The energy levels of **m-Rbs** are matched by the HOMO and LUMO orbitals (A); Molecular electrostatic potential of **m-Rbs** (B3LYP+6311G) (B); Molecular docking of **m-Rbs** with 1CBJ, 1TGU, 2X08, and $6CR_2$: three-dimensional structural diagrams (C-F) and two-dimensional interaction plots (G-J).

3.7 Molecular docking analysis

CYP51 serves as the core enzyme in the ergosterol biosynthetic pathway and plays an indispensable regulatory role in fungal metabolism. Meanwhile, superoxide dismutase (SOD), peroxidase (POD), and catalase (CAT) collectively form the intracellular antioxidant defense system, which is primarily responsible for scavenging reactive oxygen species (ROS) generated during metabolic processes.[3,45] Molecular docking analysis revealed that compound m-Rbs exhibits strong binding affinity with four target proteins (1CBJ, 1TGU, 2X08, and $6CR_2$), with binding free energies of -5.4, -8.2, -8.5, and -12.4 kcal/mol, respectively.

Compound **m-Rbs** primarily forms single hydrophobic interactions with VAL-5 and LYS-9 residues of receptor protein 1CBJ, while establishing dual hydrophobic interactions with VAL-146. For protein 1TGU, it exhibits single hydrophobic interactions with residues ALA-380, HIS-413 and GLN-414, and dual hydrophobic interactions at VAL-382. In the case of 2X08, **m-Rbs** forms single hydrophobic contacts with LYS-59, GLU-267 and LYS-268, complemented by dual hydrophobic bonds at TRP-57. With receptor 6CR2, the compound exhibits extensive single hydrophobic interactions with residues LEU-125, PHE-130, LEU-143, LYS-147, ALA-303, ALA-307, ILE-464 and LEU-503, while forming dual hydrophobic bonds with residues TYR-122, TYR-136, PHE-234 and PHE-504.

Table 2: Toxicity analysis of **m-Rbs**.

m-Rbs (μg/mL)		Number of deaths per day							Number of dead animals	Mortality (%)	LD_{50} (mg/kg)	Equivalent to the lethal dose of a person
		1d	2d	3d	4d	5d	6d	7d				
Male	25000	0	0	0	2	2	-	-	4	100	6484.198	500 g/person
	12500	0	0	0	1	1	1	0	3	75		
	6250	0	0	0	0	0	0	1	1	25		
	3125	0	0	0	0	0	0	0	0	0		
	0	0	0	0	0	0	0	0	0	0		
Female	25000	0	0	1	2	1	-	-	4	100		
	12500	0	0	0	1	2	0	0	3	75		
	6250	0	0	0	0	0	1	1	2	50		
	3125	0	0	0	0	0	0	0	0	0		
	0	0	0	0	0	0	0	0	0	0		

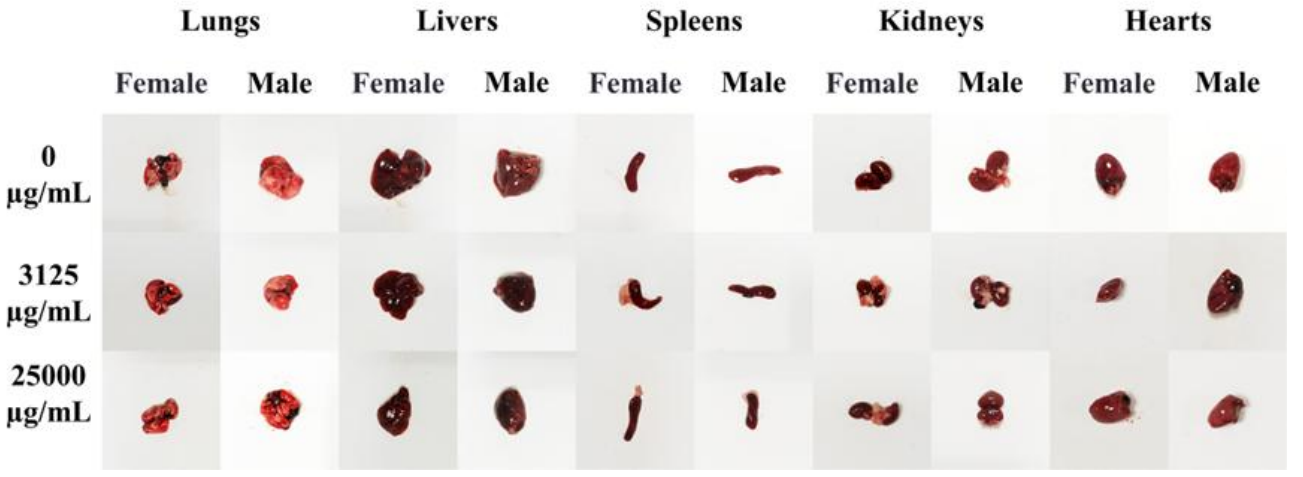

Fig. 5: Microscopic images of various organs in mice following oral administration of **m-Rbs** at different concentrations are shown here.

3.8 The toxicity of m-Rbs in mice

Evaluation of **m-Rbs** toxicity in humans based on mouse toxicity assessment, the experimental results in Table 2 showed that **m-Rbs** exhibited extremely low toxicity in mice, with a median lethal dose (LD_{50}) of 6484.198 mg/kg. According to the GB 15193.3-2014 standard, **m-Rbs** is classified as practically non-toxic, and the estimated lethal dose for an average human is approximately 500 g/person. When administered by oral gavage at 3125 μg/mL for 7 days, no mortality was observed in mice, with only body weight reduction but normal activity levels. In contrast, administration of 25000 μg/mL for 7 days resulted in 100% mortality. Fig. 5 shows anatomical images of organs from the blank control group and from the group receiving two concentrations of **m-Rbs**. The results showed that in the 3125 μg/mL group, only the liver, spleen, and heart showed slight darkening in color, while other organs showed no significant color changes or pathological lesions. The 25000 μg/mL group displayed more pronounced darkening in all organs except the heart, although no obvious pathological lesions were observed. These results indicate that **m-Rbs** can be safely used as an agricultural fungicide.

4. Conclusion

The three rosin-based quaternary ammonium salts (**o-Rbs**, **m-Rbs** and **p-Rbs**) exhibited excellent in vitro antifungal activity against five plant-pathogenic fungi. Their efficacy was comparable to or superior to that of **BAB**. Among these rosin-based quaternary ammonium salts, **m-Rbs** exhibited significant and persistent antifungal activity against all five test fungal pathogens. *In vivo* experiments demonstrated that **m-Rbs** significantly inhibit *V. mali* growth on apples. In addition, spectroscopic techniques, cellular content leakage, cell membrane permeability, DFT calculations and molecular docking revealed that **m-Rbs** disrupts normal hyphal growth by compromising membrane integrity and organelle structure. This leads to increased membrane permeability, triggering the leakage of intracellular substances and electrolytes, as well as interfering with cellular physiological activities. Additionally, by interfering with the activity of SOD, POD and CAT, **m-Rbs** disrupts the scavenging of reactive oxygen species, ultimately impairing normal cellular function. Mouse toxicological

assessment revealed an LD_{50} of 6484.198 mg/kg for **m-Rbs**, indicating its non-toxicity to humans and full compliance with safety standards. Taken together, these findings provide crucial evidence for developing novel, highly effective and non-toxic quaternary ammonium antifungal agents.

Acknowledgments
This work was supported by National Key R&D Program Funded Projects (2024YFD2201300); National Natural Science Foundation of China (32160414, 32460369, 32160351); Yunnan Agricultural Joint Project (202301BD070001-007, 202101BD070001-014); Xingdian Industrial Talent Support Plan (YNQR-CYRC-2019-012).

Conflict of Interest
The authors declare no conflict of interest.

Supporting Information
Applicable.

CRediT Statement
Chaoji Xiong: Writing – Review and editing, Writing – Original draft, Validation, Investigation, Data curation. **Bin Wu:** Writing – Review and editing, Writing – Original draft, Validation, Investigation. **Zhuo Xu:** Validation, Methodology, Investigation. **Kun Liang, Jia Deng, Zefeng Wang and Xiaoping Rao:** Validation, Methodology. **Wei Wu:** Validation, Supervision, Conceptualization, Software. **Qian Chen:** Writing – Review and editing, Validation, Methodology, Investigation, Formal analysis, Conceptualization. **Chunhua Wu:** Writing – Review and editing, Supervision, Project administration, Funding acquisition.

References
[1] M. C. Fisher, D. A. Henk, C. J. Briggs, J. S. Brownstein, L. C. Madoff, S. L. McCraw, S. J. Gurr, Emerging fungal threats to animal, plant and ecosystem health, *Nature*, 2012, **484**, 186-194, doi: 10.1038/nature10947.
[2] H. N. Fones, D. P. Bebber, T. M. Chaloner, W. T. Kay, G. Steinberg, S. J. Gurr, Threats to global food security from emerging fungal and oomycete crop pathogens, *Nature Food*, 2020, **1**, 332-342, doi: 10.1038/s43016-020-0075-0.
[3] R. Xu, K. Chen, X. Han, Y. Lou, S. Gu, Y. Gao, S. Shang, Z. Song, J. Song, J. Li, Design and synthesis of antifungal candidates containing triazole scaffold from natural rosin against *Valsa mali* for crop protection, *Journal of Agricultural and Food Chemistry*, 2023, **71**, 9718-9727, doi: 10.1021/acs.jafc.3c02002.
[4] A. de Jesús Cenobio-Galindo, A. D. Hernández-Fuentes, U. González-Lemus, A. K. Zaldívar-Ortega, L. González-Montiel, A. Madariaga-Navarrete, I. Hernández-Soto, Biofungicides based on plant extracts: on the road to organic farming, *International Journal of Molecular Sciences*, 2024, **25**, 6879, doi: 10.3390/ijms25136879.
[5] S. Mao, C. Wu, Y. Gao, J. Hao, X. He, P. Tao, J. Li, S. Shang, Z. Song, J. Song, Pine rosin as a valuable natural resource in the synthesis of fungicide candidates for controlling *Fusarium oxysporum* on cucumber, *Journal of Agricultural and Food Chemistry*, 2021, **69**, 6475-6484, doi: 10.1021/acs.jafc.1c01887.
[6] M. C. Fisher, N. J. Hawkins, D. Sanglard, S. J. Gurr, Worldwide emergence of resistance to antifungal drugs challenges human health and food security, *Science*, 2018, **360**, 739-742, doi: 10.1126/science.aap7999.
[7] Y.-X. Wang, Y. Ye, Z.-W. Li, G.-R. Cui, X.-X. Shi, Y. Dong, J.-J. Jiang, J.-Y. Sun, Z.-W. Guan, N. Zhang, Q.-Y. Wu, F. Wang, X.-L. Zhu, G.-F. Yang, Cryo-EM structures reveal the unique binding modes of metyltetraprole in yeast and porcine cytochrome bc_1 complex enabling rational design of inhibitors, *Journal of the American Chemical Society*, 2024, **146**, 33903-33913, doi: 10.1021/jacs.4c12595.
[8] X. He, K. Jia, L. Yu, H. Li, J. Xin, X. Zheng, J. Ning, H. Wu, L. Huang, W. Wen, Robust pH-switchable Pickering emulsions stabilized solely by organic Rosin-based particles with adjustable wettability, *Journal of Molecular Liquids*, 2022, **353**, 118751, doi: 10.1016/j.molliq.2022.118751.
[9] X.-M. Cai, Z. Tang, X. Chen, Y. Lin, X. Zhang, S. Huang, Construction of two rosin-based BioAIEgens with distinct fluorescence and mechanochromic propertites for rewritable paper, *Dyes and Pigments*, 2022, **204**, 110454, doi: 10.1016/j.dyepig.2022.110454.
[10] F. Zhao, W. Lu, Y. Xu, L. Xu, J. Zhang, X. Sun, S. Yang, M. Zhou, F. Su, F. Lin, F. Cao, Synthesis and high antiproliferative activity of dehydroabietylamine pyridine derivatives *in vitro* and *in vivo*, *Biochemical Journal*, 2020, **477**, 2383-2399, doi: 10.1042/bcj20200337.
[11] J. Yan, Y. Zhu, G. Hu, Q. Liang, L. Ge, K. Yang, Chiral quaternary ammonium ionic liquids derived from natural dehydroabietylamine and their potential application in chiral molecular recognition, *Tetrahedron*, 2023, **130**, 133165, doi: 10.1016/j.tet.2022.133165.
[12] M. A. Dea-Ayuela, P. Bilbao-Ramos, F. Bolás-Fernández, M. A. González-Cardenete, Synthesis and antileishmanial activity of C7- and C12-functionalized dehydroabietylamine derivatives, *European Journal of Medicinal Chemistry*, 2016, **121**, 445-450, doi: 10.1016/j.ejmech.2016.06.004.
[13] J. Wiemann, A. Loesche, R. Csuk, Novel dehydroabietylamine derivatives as potent inhibitors of acetylcholinesterase, *Bioorganic Chemistry*, 2017, **74**, 145-157, doi: 10.1016/j.bioorg.2017.07.013.
[14] H. Feng, Y. Pan, Y. Zhang, Z. Zhang, Y. Huang, L. Hou, L. Xiao, Surface activity and cleaning performance of rosin-based quaternary ammonium salt type asymmetric Gemini surfactants, *Chinese Journal of Chemical Engineering*, 2024, **73**, 70-80, doi: 10.1016/j.cjche.2024.05.004.
[15] V. C. Roa-Linares, Y. M. Brand, L. S. Agudelo-Gomez, V. Tangarife-Castaño, L. A. Betancur-Galvis, J. C. Gallego-Gomez, M. A. González, Anti-herpetic and anti-dengue activity of abietane ferruginol analogues synthesized from (+)-dehydroabietylamine, *European Journal of Medicinal Chemistry*, 2016, **108**, 79-88, doi: 10.1016/j.ejmech.2015.11.009.

[16] S.-G. Zhang, Y.-Q. Wan, W.-H. Zhang, Discovery of dehydroabietylamine derivatives as antibacterial and antifungal agents, *Journal of Natural Products*, 2024, **87**, 924-934, doi: 10.1021/acs.jnatprod.3c01213.
[17] Z. Yang, Q. Liu, Y. Sun, X. Sun, L. Sun, L. Chen, W. Gu, Novel aromatic carboxamides from dehydroabietylamine as potential fungicides: Design, synthesis and antifungal evaluation, *Arabian Journal of Chemistry*, 2022, **15**, 104330, doi: 10.1016/j.arabjc.2022.104330.
[18] J. Wang, F. Liu, Q. Peng, X. Zhang, Z. Gao, P. Zhang, W. Wang, J. Sun, Unveiling solubilization mechanisms of natural deep eutectic solvents in triazole fungicides: COSMO-RS calculations and screening for eco-friendly, high-efficiency pesticide systems, *ACS Sustainable Chemistry & Engineering*, 2024, **12**, 13149-13162, doi: 10.1021/acssuschemeng.4c03110.
[19] B.-I. Andreica, X. Cheng, L. Marin, Quaternary ammonium salts of chitosan. A critical overview on the synthesis and properties generated by quaternization, *European Polymer Journal*, 2020, **139**, 110016, doi: 10.1016/j.eurpolymj.2020.110016.
[20] Z. Zhou, X. Zhang, S. Zeng, Y. Xu, W. Nie, Y. Zhou, P. Chen, Quaternary ammonium salts for water treatment with balanced rate of sterilization and degradation, *Chemosphere*, 2024, **352**, 141386, doi: 10.1016/j.chemosphere.2024.141386.
[21] X. Zhang, H. Kong, X. Zhang, H. Jia, X. Ma, H. Miao, Y. Mu, G. Zhang, Design and production of environmentally degradable quaternary ammonium salts, *Green Chemistry*, 2021, **23**, 6548-6554, doi: 10.1039/d1gc01525g.
[22] A. Morandini, E. Spadati, B. Leonetti, R. Sole, V. Gatto, F. Rizzolio, V. Beghetto, Sustainable triazine-derived quaternary ammonium salts as antimicrobial agents, *RSC Advances*, 2021, **11**, 28092-28096, doi: 10.1039/d1ra03455c.
[23] B. Nunes, F. Cagide, F. Borges, M. Simões, Antimicrobial activity and cytotoxicity of novel quaternary ammonium and phosphonium salts, *Journal of Molecular Liquids*, 2024, **401**, 124616, doi: 10.1016/j.molliq.2024.124616.
[24] G. Pan, Q. Wang, H. Ding, J. Deng, S. Gao, L. Wang, Turning dextran into antibacterial fibers: quaternary ammonium salt for antibacterial treatment and wound healing, *Arabian Journal of Chemistry*, 2024, **17**, 105771, doi: 10.1016/j.arabjc.2024.105771.
[25] J. Zhang, W. Tan, F. Luan, X. Yin, F. Dong, Q. Li, Z. Guo, Synthesis of quaternary ammonium salts of chitosan bearing halogenated acetate for antifungal and antibacterial activities, *Polymers*, 2018, **10**, 530, doi: 10.3390/polym10050530.
[26] L. Wei, W. Tan, G. Wang, Q. Li, F. Dong, Z. Guo, The antioxidant and antifungal activity of chitosan derivatives bearing Schiff bases and quaternary ammonium salts, *Carbohydrate Polymers*, 2019, **226**, 115256, doi: 10.1016/j.carbpol.2019.115256.
[27] Y. H. Kim, K. S. Yoon, S.-J. Lee, E.-J. Park, J.-W. Rhim, Synthesis of fully deacetylated quaternized chitosan with enhanced antimicrobial activity and low cytotoxicity, *Antibiotics*, 2022, **11**, 1644, doi: 10.3390/antibiotics11111644.
[28] H. Kono, Y. Sogame, U.-E. Purevdorj, M. Ogata, K. Tajima, Bacterial cellulose nanofibers modified with quaternary ammonium salts for antimicrobial applications, *ACS Applied Nano Materials*, 2023, **6**, 4854-4863, doi: 10.1021/acsanm.3c006
[29] L. Liao, Z. Ke, X. Wang, S. Li, S. Wang, X. Rao, Recyclable ethyl cellulose film modified by rosin based quaternary ammonium salt for antimicrobial packaging, *Industrial Crops and Products*, 2023, **198**, 116692, doi: 10.1016/j.indcrop.2023.116692.
[30] Y. Zhou, Y. Jiang, Y. Zhang, L. Tan, Improvement of antibacterial and antifouling properties of a cellulose acetate membrane by surface grafting quaternary ammonium salt, *ACS Applied Materials & Interfaces*, 2022, **14**, 38358-38369, doi: 10.1021/acsami.2c09963.
[31] L. An, J. W. Heo, J. Chen, Y. S. Kim, Water-soluble lignin quaternary ammonium salt for electrospun morphology-controllable antibacterial polyvinyl alcohol/lignin quaternary ammonium salt nanofibers, *Journal of Cleaner Production*, 2022, **368**, 133219, doi: 10.1016/j.jclepro.2022.133219.
[32] M. K. Mohan, H. Kaur, M. Rosenberg, E. Duvanova, T. Lukk, A. Ivask, Y. Karpichev, Synthesis and antibacterial properties of novel quaternary ammonium lignins, *ACS Omega*, 2024, **9**, 39134-39145, doi: 10.1021/acsomega.4c06000.
[33] Y. Ma, J. Dai, L. Wu, G. Fang, Z. Guo, Enhanced anti-ultraviolet, anti-fouling and anti-bacterial polyelectrolyte membrane of polystyrene grafted with trimethyl quaternary ammonium salt modified lignin, *Polymer*, 2017, **114**, 113-121, doi: 10.1016/j.polymer.2017.02.083.
[34] Y. Lin, C. Zhang, M. Hou, R. Li, A. Zhang, Polymeric diallyl quaternary ammonium salts for inhibiting banana Fusarium wilt, *Reactive and Functional Polymers*, 2022, **172**, 105174, doi: 10.1016/j.reactfunctpolym.2022.105174.
[35] B. Wu, C. Xiong, Z. Xu, K. Liang, C. Wu, W. Wu, Q. Chen, Renewable rosin-based bisquaternary ammonium salt with pyridyl design, synthesis and antifungal activity, *Food Chemistry*, 2025, **482**, 144188, doi: 10.1016/j.foodchem.2025.144188.
[36] A.-L. Bao, X.-S. Xie, D.-Y. Wang, Z.-Q. Deng, Y. Chen, D. Liu, W.-Y. Li, X.-R. Tang, W. Cheng, Y.-K. Yan, Design, synthesis and antifungal activity of novel pyrazole-amide-isothiazole derivatives as succinate dehydrogenase inhibitors, *Food Chemistry*, 2025, **464**, 141465, doi: 10.1016/j.foodchem.2024.141465.
[37] R. Xu, Y. Kong, Y. Lou, J. Wu, Y. Gao, S. Shang, Z. Song, J. Song, J. Li, Design, synthesis and biological activity evaluation of eco-friendly rosin-based fungicides for sustainable crop protection, *Pest Management Science*, 2024, **80**, 5898-5908, doi: 10.1002/ps.8323.
[38] D. Ma, D. Ji, Z. Zhang, B. Li, G. Qin, Y. Xu, T. Chen, S. Tian, Efficacy of rapamycin in modulating autophagic activity of Botrytis cinerea for controlling gray mold, *Postharvest Biology and Technology*, 2019, **150**, 158-165, doi: 10.1016/j.postharvbio.2019.01.005.
[39] Y. Yan, S. Liu, L. An, Y. Yang, G. Tian, X. Bao, Synthesis, crystal structure, and antimicrobial evaluation of novel 4-oxyquinazoline derivatives containing a benzimidazole moiety, *Journal of Molecular Structure*, 2024, **1303**, 137611, doi: 10.1016/j.molstruc.2024.137611.

[40] Y. Gao, R. Xu, S. Gu, K. Chen, J. Li, X. He, S. Shang, Z. Song, J. Song, Discovery of natural rosin derivatives containing oxime ester moieties as potential antifungal agents to control tomato gray mold caused by *Botrytis cinerea*, *Journal of Agricultural and Food Chemistry*, 2022, **70**, 5551-5560, doi: 10.1021/acs.jafc.2c01532.

[41] X.-D. Yin, K.-Y. Ma, Y.-L. Wang, Y. Sun, X.-F. Shang, Z.-M. Zhao, R.-X. Wang, Y.-J. Chen, J.-K. Zhu, Y.-Q. Liu, Design, synthesis, and antifungal evaluation of 8-hydroxyquinoline metal complexes against phytopathogenic fungi, *Journal of Agricultural and Food Chemistry*, 2020, **68**, 11096-11104, doi: 10.1021/acs.jafc.0c01322.

[42] Z. Xu, B. Wu, C. Wu, Q. Chen, K. Xu, Z. Shi, X. Rao, Y. Niu, Antifungal properties and preservation applications of resin acid modified chitosan derivatives, *Food Bioscience*, 2025, **66**, 106204, doi: 10.1016/j.fbio.2025.106204.

[43] C. Xiong, S. F. University, X. Zhang, S. F. University, K. Liang, S. F. University, C. Wu, S. F. University, W. Wu, X. Rao, H. University, Q. Chen, S. F. University, Thiophene-based porous triazine polyamide (Tb-PTPa) as the next promising and cost-effective eliminator of Hg^{2+} in aqueous media, *ACS Applied Materials & Interfaces*, 2025, **17**, 13970-13979, doi: 10.1021/acsami.4c21158.

[44] C. Xiong, H. Wang, Z. Zhang, K. Liang, C. Wu, W. Wu, X. Rao, Q. Chen, Triazine-based sulphur-containing polymers for Hg^{2+} adsorption: efficiency and mechanism, *Polymer*, 2023, **289**, 126480, doi: 10.1016/j.polymer.2023.126480.

[45] L. Garnier, M. Penland, A. Thierry, M.-B. Maillard, J. Jardin, M. Coton, M. Leyva Salas, E. Coton, F. Valence, J. Mounier, Antifungal activity of fermented dairy ingredients: Identification of antifungal compounds, *International Journal of Food Microbiology*, 2020, **322**, 108574, doi: 10.1016/j.ijfoodmicro.2020.108574.

[46] L. Li, Y. Xu, Z. Xu, C. Wu, Q. Chen, K. Xu, Z. Shi, X. Rao, Synthesis, characterization and antifungal properties of maleopimaric anhydride modified chitosan, *International Journal of Biological Macromolecules*, 2024, **267**, 131373, doi: 10.1016/j.ijbiomac.2024.131373.

[47] Z. Xu, B. Wu, C. Wu, Q. Chen, Y. Niu, Z. Shi, K. Liang, X. Rao, Acrylpimaric acid-modified chitosan derivatives as potential antifungal agents against Valsa Mali, *Carbohydrate Polymers*, 2025, **352**, 123244, doi: 10.1016/j.carbpol.2025.123244.

[48] S. J. Marrink, V. Corradi, P. C. T. Souza, H. I. Ingólfsson, D. P. Tieleman, M. S. P. Sansom, Computational modeling of realistic cell membranes, *Chemical Reviews*, 2019, **119**, 6184-6226, doi: 10.1021/acs.chemrev.8b00460.

[49] Y. Peng, B. Chen, Role of cell membrane homeostasis in the pathogenicity of pathogenic filamentous fungi, *Virulence*, 2024, **15**, 22991836, doi: 10.1080/21505594.2023.2299183.